ACS Catalysis

Research Article

pubs.acs.org/acscatalysis

Photo-Oxidation of Water on Defective Hematite(0001)

Manh-Thuong Nguyen,*[,†] Simone Piccinin,[‡] Nicola Seriani,[†] and Ralph Gebauer[†]

[†]The Abdus Salam International Centre for Theoretical Physics, Strada Costiera 11, 34151 Trieste, Italy

[‡]CNR-IOM DEMOCRITOS, c/o SISSA, Via Bonomea 265, 34136 Trieste, Italy

Supporting Information

ABSTRACT: Defects are unavoidable and usually originate exotic properties in realistic materials. One of the most fundamental defect-induced properties of a solid surface is its reactivity to adsorbed species. Defects in anodes of electrochemical cells for water splitting could therefore play a critical role in the interatomic interactions at the solvent/solid interfaces and hence in determining the catalytic properties of these materials. Here, by means of density-functional calculations at the PBE+U level, we investigate photo-oxidation of water on defective hematite(0001) substrates which accommodate intrinsic and extrinsic point defects, namely, Fe and O vacancies, as well as N substitutional impurities. In this work, the water oxidation process is assumed to be driven by the redox potential for photogenerated holes with respect to the normal hydrogen electrode. Although iron vacancies do not reduce the overpotential, oxygen vacancies and N impurities lower the overpotential by 0.2−0.3 V compared to the ideal case. These changes are attributed to the coordination loss or the substitution-induced charge states of surface atoms that modify the electronic structure of the surface, thus affecting the relative stability of adsorbed intermediates.

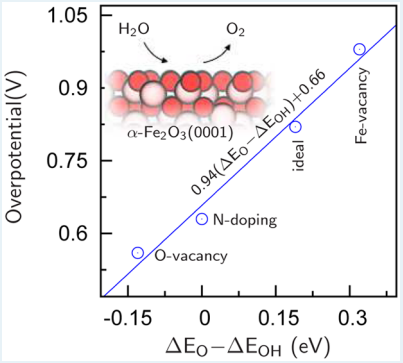

KEYWORDS: *water oxidation, hematite, surface defects, density functional theory, molecule−surface interactions*

1. INTRODUCTION

The enormous increase in demand for energy in recent years has become a global problem, and the quest for cheap, clean, renewable energy resources is increasingly urgent. The development of efficient ways to exploit the energy from the sun is an issue of major importance. Among possible solutions, the employment of solar energy to promote chemical reactions has the advantage of addressing the problems of harvesting, converting and storing energy at the same time. In this context, water splitting plays a central role, both for direct hydrogen production and for the production of hydrocarbons. Therefore, great attention has been recently devoted to hydrogen production by means of photoelectrochemical (PEC) cells, via water splitting to molecular hydrogen and oxygen, $2H_2O \rightarrow 2H_2 + O_2$ ($E^0 = 1.23$ V with respect to the Standard Hydrogen Electrode (SHE)).[1,2] The main challenge is to develop anode materials for these cells that can split water efficiently.

Hematite (α-Fe_2O_3, α is dropped henceforth) has emerged as a highly interesting material for photoanodes. Abundant, stable, nontoxic, and, importantly, possessing an energy gap of 2.1 eV, Fe2O3 has been intensively investigated in numerous experiments, often focusing on its photocatalytic properties.[2,3] However, Fe_2O_3 still suffers from drawbacks such as low conductivity and slow reaction kinetics, so far hindering its use in real photoelectrochemical (PEC) cells. The overpotential of 0.5−0.6 V is also a major shortcoming.[2,27] Recent studies considered the possibility of doping to improve the performance of Fe_2O_3,[2,4] but the generation of oxygen vacancies could be exploited.[5]

Vacancies in metal oxides are, like any other defects, partly responsible for modifications of physical properties of the crystals.[6] Eliminating atoms from a metal oxide surface results in the formation of extra dangling bonds; as a result, vacancies usually change the chemical reactivity of the surface.[7,8] Replacing a native atom in the lattice with a foreign counterpart also changes the electronic states of surrounding atoms. Not surprisingly, metal substitutional impurities on metal oxide surfaces alter adsorption energies.[4,9] Given that vacancies/impurities can be intentionally or unintentionally generated in sample preparation processes, understanding their influence on the oxidation of water at anodes of electrochemical cells is desirable, for both scientific and technological reasons.

Owing to the significant rise of interest in Fe_2O_3 as a photocatalyst for water oxidation, in this work, by means of density functional theory (DFT) calculations, we investigate the effects of vacancies and impurities on water photo-oxidation on hematite(0001) surfaces. It has recently been demonstrated that oxygen vacancies can remarkably activate the photoactivity of pure Fe_2O_3.[5] Dopants, on the other hand, can improve the conductivity of this material.[10] The combination of these two kinds of defects significantly enhances the water splitting performance of Fe_2O_3.[5] In this work, we considered O and Fe vacancies, and nonmetal impurities, namely, N replacing O. We show that *first-principles* methods are able to rationalize the

Received: August 18, 2014
Revised: December 15, 2014
Published: December 16, 2014

DOI: 10.1021/cs5017326
ACS Catal. 2015, 5, 715−721

positive effect of oxygen vacancies on water splitting. Moreover, we predict that doping by N should have a similarly positive effect. In the literature, *first-principles* studies were focused on metal substituents.[4] To our knowledge, doping of hematite with a single nonmetal element for water splitting has not been experimentally investigated. Fabrication and photocatalytic activity of S and N codoped hematite structures, on the other hand, has been reported.[11] Starting from the thermodynamically most stable surface for water photooxidation of Fe_2O_3 (0001), namely, the fully oxygenated double iron termination (O_3−Fe−Fe−),[12] vacancies/impurities are introduced by removing/replacing surface atoms from/with the surface/N. Given that surface oxygen can be a key player in the water oxidation process, an oxygen vacancy in the outermost layer of the surface can be filled up by oxygen from water, the surface will therefore operate in the defect-free regime. For this reason, we consider oxygen vacancies in the second layer, while those in deeper position are assumed to be less effective.

2. METHODOLOGY AND MODELS

The four-electron semireaction of water oxidation leads to the formation of molecular oxygen. Direct combination of adsorbed oxygen atoms creating oxygen molecules could in principle be possible, however, it has been shown that this route has high activation energy[21] or exceedingly high overpotentials.[12] A more widely accepted mechanism involves the formation of a hydroperoxo group HOO* from the nucleophilic attack of a solvent water molecule on an oxygen adsorbate. As described in previous studies,[12,21−24] this water oxidation mechanism consists of a series of four proton-coupled electron transfer (PCET) steps

$$\begin{aligned} 2H_2O + ()^* &\xrightarrow{A} HO^* + H_2O + H^+ + e^- \\ &\xrightarrow{B} O^* + H_2O + 2(H^+ + e^-) \\ &\xrightarrow{C} HOO^* + 3(H^+ + e^-) \\ &\xrightarrow{D} O_2 + 4(H^+ + e^-) + ()^* \end{aligned} \quad (1)$$

where ()* indicates an active surface site (i.e., an undercoordinated surface Fe atom) and A, B, C, D label reaction steps.[12] To calculate the reaction free energy for each step, we adopt the theoretical scheme introduced by Nørskov and coworkers.[22] Briefly, when the equilibrium $1/2\ H_2 \rightleftharpoons H^+ + e^-$ at $p(H_2)$ =1 bar and T = 298 K is established, the SHE potential is set to be the reference potential, and has, by definition, an electrode potential $U_b = 0$. The chemical potentials of electrons and protons for a PCET do not need to be known separately, and using the SHE as reference, their sum can be taken to be equal to the chemical potential of gas phase hydrogen, which can be straightforwardly computed. At a set of standard conditions (U_b = 0, pH = 0, p = 1 bar, T = 298 K) the reaction energy free energy of HA* → A + H^+ + e^- can accordingly be calculated as that of HA* → A + 1/2H_2. The chemical potential of the electrons and of the protons is changed by $-eU_b$ and $-k_BT\ln(10) \times$ pH in the presence of external bias U_b (against the SHE) and pH, respectively. Consequently, the reaction free energy of a PCET step is computed as

$$\Delta G(U_b, \text{pH}) = \Delta E + (\Delta\text{ZPE} - T\Delta S) - eU_b - k_BT\ln(10) \times \text{pH} \quad (2)$$

where ΔE is the reaction energy, ΔZPE is the zero-point energy change, and ΔS is the entropy change. In this work, the values of ZPE and S are taken from ref 23 (see Table 1). The effect of solar illumination, the driving force for the oxidation, is the creation of holes at the valence band maximum of hematite. Exploiting the experimental evidence that the conduction band of hematite is at about 0.2 V with respect to NHE and the band gap is 2.1 eV, the photogenerated holes provide at effective bias of 2.3 V.[23] The pH dependence refers to the reaction in this half-cell; still, the pH might have an effect also on the other half-cell and on the band edges of hematite. It is therefore not trivial to evaluate the pH-dependence of the overall cell reactions (see, for example, ref 13 for an account), and the fact that pH can also affect the onset of the water oxidation reactions on hematite photoanodes;[29,30] however, analyzing the pH-dependence goes beyond the scope of this paper.

Table 1. Zero Point Energy and Entropic Contributions to the Free Energy, Data Taken from Ref 23

species	ZPE (eV)	TS (eV)	ZPE-TS (eV)
H_2	0.33	0.41	−0.08
O_2	0.10	0.64	−0.54
H_2O	0.58	0.67	−0.09
O*	0.07	0.02	0.05
HO*	0.37	0.03	0.34
HOO*	0.44	0.06	0.38

The energetics was calculated using spin-polarized plane-wave density functional theory, at the PBE+U level of theory,[14,15] in which the effective Coulomb repulsion parameter, U, for Fe was set at 4.2 eV, as implemented in the Quantum ESPRESSO package.[16] It is known that the localized nature of the Fe 3d states in Fe_2O_3 is not necessarily well described by PBE (or DFT in general). To obtain more accurate electronic properties of hematite, more sophisticated methods like DFT+U[17] are necessary. We use here a value of U of 4.2 eV, because it leads to an energy gap of about 2.0 eV in our calculations.[20]

The interactions between the electrons and ions were represented with ultrasoft pseudopotentials.[18,19] We employed a kinetic energy cutoff of 40 Ry for the wave function and 400 Ry for the charge density. The force convergence threshold was set at 0.001 a.u for geometry optimizations. The charge distribution at the surface has been analyzed by means of Bader's Atom-in-Molecule theory,[25] as implemented in the code by Henkelman and co-workers.[26]

As shown in previous works,[12,23] upon solar illumination we can consider the O_3−Fe−Fe− termination as the starting surface in the water oxidation circle. In this work, this termination is what we consider as the ideal defect-free surface. To model the surface, we use slabs with a 2 × 2 (10.14 × 10.14 Å ^{2}) surface unit cell, using three iron and four oxygen layers (see Figure 1a) with antiferromagnetic ordering. The slabs here are slightly thinner than ones employed in our previous work (five iron + six oxygen layers), but this modification leads to changes in the overpotential of just 0.02 V, which for our purposes is negligibly small. Iron vacancies were generated by eliminating iron atoms in the slab, and three different vacancy sites (associated with iron atoms labeled X, Y, Z in Figure 1b) were investigated. An oxygen vacancy in the second layer was considered. Finally, as the starting surface is fully terminated with oxygen, the PCET steps ordering is C → D → A → B.

DOI: 10.1021/cs5017326
ACS Catal. 2015, 5, 715−721

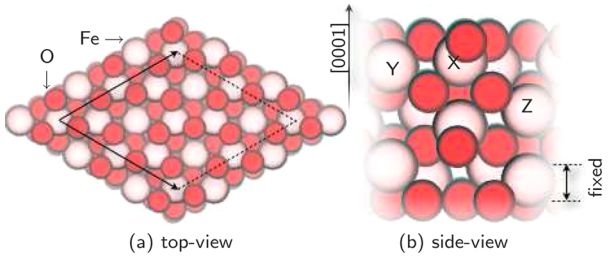

Figure 1. (a) 2 × 2 surface unit cell indicated by arrows, O in red and Fe in pink. (b) Iron atoms in the outermost layer marked with X and Y, in the second layer with Z, the fixed O−Fe layer indicated with "fixed".

3. RESULTS AND DISCUSSION

3.1. Oxygen Vacancy. As explained in Section 1, because oxygen vacancy defects in the outermost layer of the hematite surface would be healed in water oxidation processes, we now consider a vacancy in a position deeper within the slab. Each oxygen atom in the second layer, which is sandwiched between two iron layers, is coordinated to four iron atoms. Eliminating an oxygen atom from this layer leaves two iron atoms in the topmost layer under-coordinated. In the absence of the oxygen atom, the space around these two iron atoms, labeled X_1 and Y_1 in Figure 2a, is considerably modified with respect to the pristine surface. Although neighboring Fe−Fe bonds are almost unchanged, X_1Y_1 is elongated by 0.4 Å.

Figure 2b shows the energetics of the water oxidation process on the ideal and oxygen-vacancy surfaces. Because the starting surface is fully terminated with oxygen, this corresponds to the presence of the O* intermediate. Step C leads to the formation of an hydroperoxo group, which requires the dissociation of a water molecule and the transfer of a proton to the electrolyte. In step D, molecular oxygen is formed, a proton is transferred to the electrolyte, leaving two Fe surface atoms under-coordinated. This is followed by step A, in which a second water molecule comes into play, coordinating the Fe sites and transferring one of its protons to the electrolyte. Finally, the surface releases the remaining proton, closing the circle. At zero bias, the maximum free energy change in this circle is 2.05 eV (step B), corresponding to the overpotential of 0.82 V. Note that the overpotential computed for the (2 × 2) surface unit cell is almost identical to the one computed on the (1 × 1) surface unit cell, 0.81 eV. The second most demanding step is C, 1.31 eV, while the least demanding is step D, 0.38 eV.

The water oxidation process on the oxygen-vacancy surface under consideration proceeds in a similar fashion. The change in free energy associated with each step, however, is considerably different. Without external bias, step C now becomes the most demanding, with a free energy cost of 1.79 eV, while step B requires 1.73 eV. Hence, the overpotential is in this case 0.56 V, substantially lower than in the case of the pristine surface. Thus, the calculations are able to reproduce and rationalize the fact, observed experimentally, that oxygen vacancies have a positive effect on the activity of hematite for water splitting.[5] This is a confirmation of the power of the methods we use, and gives more weight to the prediction, reported in the next section, that also N-doping has a positive effect on the activity of hematite.

Moreover, because from the calculations we can also extract the nature of the reaction step that determines the overpotential (B for the ideal surface and C for the surface with and oxygen defect), we can also rationalize the origin of the lowering of the overpotential induced by the presence of O-vacancies, by writing down the energetics of step B:

$$\mathrm{HO^*} \xrightarrow{\mathrm{B}} \mathrm{O^*} + (\mathrm{H^+} + e^-)$$

$$\Delta G_B = E_{\mathrm{O^*}} + \frac{1}{2}E_{\mathrm{H_2}} - E_{\mathrm{HO^*}} + (\Delta\mathrm{ZPE} - \mathrm{T}\Delta S)_{\{\mathrm{HO^*}\rightarrow\mathrm{O^*}+1/2\mathrm{H_2}\}}. \quad (3)$$

Because the entropic contributions to the free energy changes are assumed to be identical in the two cases, the lowering of the overpotential is due to the changes in the adsorption energy of the HO* and O* intermediates. We therefore report in Table 2

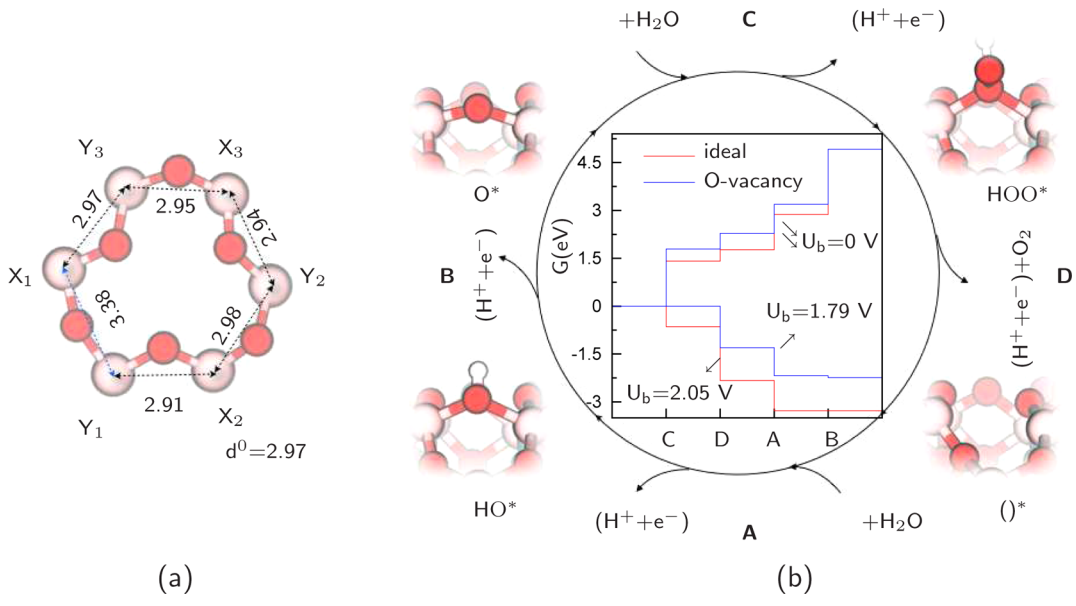

Figure 2. (a) Structure of surface atoms near the oxygen vacancy, X_1 and Y_1 are Fe atoms coordinated by the oxygen atom that was removed to create the vacancy, d^0 is X_1Y_1 bond length of the defect-free surface, bondlengths are in Å, (b) Oxygen evolution at the X_1Y_1 bridge site.

DOI: 10.1021/cs5017326
ACS Catal. 2015, 5, 715−721

the adsorption energies of the intermediates ΔE_α (α = O, OH, and OOH) on ideal and defective surfaces, calculated as

$$\Delta E_\alpha = E_{S-\alpha} - E_S - E_\alpha \quad (4)$$

where E_S is the energy of the ()* intermediate (i.e., a surface with a free site).

On the ideal and O-vacancy surfaces, $\Delta E_O - \Delta E_{OH}$ = 0.19 and −0.13 eV, respectively. The difference between the two cases here, 0.32 eV, is the origin of the change of ΔG_B caused by the vacancy (see above). Similarly, in step C, which involves the O* and HOO* intermediates, $(\Delta E_{OOH} - \Delta E_O)_{ideal} - (\Delta E_{OOH} - \Delta E_O)_{O-vacancy}$ = 1.30−1.79 = −0.49 eV, which is the defect-induced change of ΔG_C. Note that the stability of O, OH, and OOH species is enhanced with the vacancy by different magnitudes, see Table 2. To understand why the effects of the presence of a vacancy are larger on O than on OH and OOH, we now look at the electronic properties of these systems.

Table 2. Overpotential η (in V) of the Oxidation Circles, Adsorption Energy ΔE_α (in eV) of α (α = O, OH, and OOH), Partial Charge $q_{\zeta/\gamma}$ (in $|e^-|$) of Atom ζ (ζ = X,Y, and O Binding to X and Y) in Intermediate γ (γ = ()*,O*, HO*, and HOO*)

	ideal	O-va	Fe-va	N-doped
η	0.82	0.56	0.98	0.63
ΔE_O	−2.22	−2.73	−0.98	−2.21
ΔE_{OH}	−2.41	−2.60	−1.30	−2.21
ΔE_{OOH}	−0.92	−0.94	−0.54	−0.78
$q_{O/O*}$	−0.69	−0.82	−0.36	−0.63
$q_{X/O*}$	1.74	1.70		1.70
$q_{Y/O*}$	1.81	1.75	1.77	1.72
$q_{O/HO*}$	−1.41	−1.44	−1.24	−1.38
$q_{X/HO*}$	1.75	1.70		1.70
$q_{Y/HO*}$	1.82	1.73	1.80	1.76
$q_{O/HOO*}$	−0.43	−0.46	−0.16	−0.39
$q_{X/HOO*}$	1.74	1.71		1.71
$q_{Y/HOO*}$	1.79	1.72	1.79	1.73
$q_{X/()*}$	1.69	1.68		1.65
$q_{Y/()*}$	1.74	1.69	1.77	1.67

Bader analysis results, Table 2, show that the charge states the two atoms X_1 and Y_1 through the water oxidation process is lowered by the vacancy. It also appears that the change, induced by the vacancy, of partial atomic charge on the O atom in O* is more pronounced than in the HO* and HOO* intermediates. As listed in Table 2, the change in the Bader charge on the O atom in O*, HO* and HOO* is 0.13, 0.03, and 0.03 electrons, respectively. The corresponding variation in the adsorption energy of these species is 0.51, 0.19, and 0.02 eV. This analysis therefore shows that the large change in the adsorption energy of the O* intermediate correlates with the electronic charge of the oxygen atom, where an accumulation of electrons on oxygen leads to an increase of its adsorption energy.

3.2. Iron Vacancy. Each iron atom on the surface is coordinated to three oxygen atoms in the outermost layer. Removing a surface iron atom leads to three singly coordinated oxygen atoms. We considered three possible Fe vacancy sites, associated with the absence of iron atoms labeled X, Y, and Z in Figure 1, which lead to an overpotential of 0.98, 0.90, and 0.83 V, respectively. These results show that presence of an iron vacancy in the second layer (Z) does not affect the overpotential, while those in the first layer (X, Y) give rise to an increase of the overpotential. To understand the origins of this behavior, we will analyze results in the case of vacancy X.

The removal of the X atom has the effect that the surrounding O atoms become undercoordinated, because they are now only bonded to Y atoms. Figure 3 shows the four PCET steps at a Y site and associated free energies. It appears that the changes in free energy of step C and D are rather small, while steps A and B are responsible for major changes in the energetics of the reaction. Quantitatively, the reaction free energy in steps C, D, A, and B is 0.45, 0.08, 2.21, and 2.18 eV, respectively. Consequently, the overpotential in this case is 0.98 V. Comparing their free energy changes to the defect-free case, the Fe vacancy makes O, OH, OOH much less stable, resulting in an opposite effect with respect to the O vacancy.

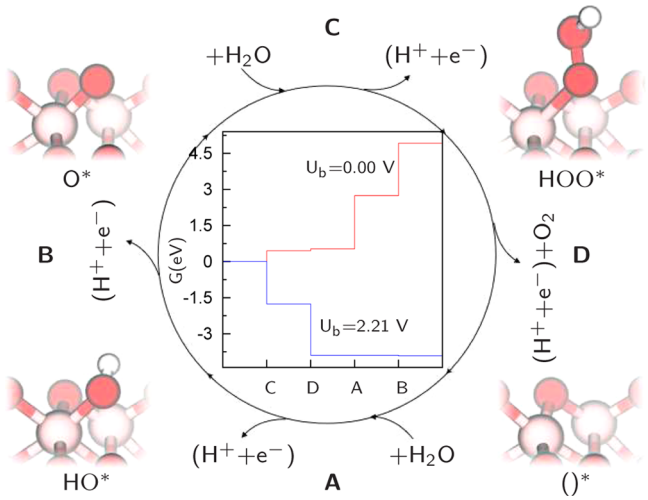

Figure 3. Oxygen evolution at an Fe-vacancy surface.

We attribute this effect to the fact that in the presence of an Fe vacancy these adsorbates bind to a single Fe atom, while on the pristine surface they are bonded to two Fe atoms. In step C, the metal vacancy effects on O is much stronger than on OOH, according to Table 2, reducing the free energy cost of this step, which depends on the quantity $\Delta E_{OOH} - \Delta E_O$. Step A, on the other hand, exhibits the opposite behavior, because the adsorption energy of OH changes from −2.41 eV in the defect-free case to −1.30 eV in the presence of an Fe vacancy.

Partial atomic charges, Table 2, show remarkable differences when compared against the ideal and O vacancy cases. In contrast to the O vacancy, the loss of a Fe bonding partner results in a strong decrease of the electron gain of the O atom in intermediate O* (i.e., the O atom is less negatively charged). The adsorption energy of O of −0.98 eV implies that it is much less stable than on the ideal or O vacancy surface. In a similar way, the O atom in intermediates HO* and HOO* is also much less negatively charged and the stability of these intermediates is considerably lower that on the pristine and O-vacancy surfaces.

3.3. N Impurities. In this section, we consider the case in which an oxygen atom in the first or second layer of the ideal surface is substituted with a N atom. For the first layer substitution, we consider an oxygen evolution process occurring at the N atom and in its vicinity. In the former case, the HO*

DOI: 10.1021/cs5017326
ACS Catal. 2015, 5, 715−721

and HOO* intermediates are unstable, while in the latter case the minimum overpotential is about 0.8 V.

Figure 4 shows the water oxidation process on the N-substitution surface in the second layer. Like in previous cases,

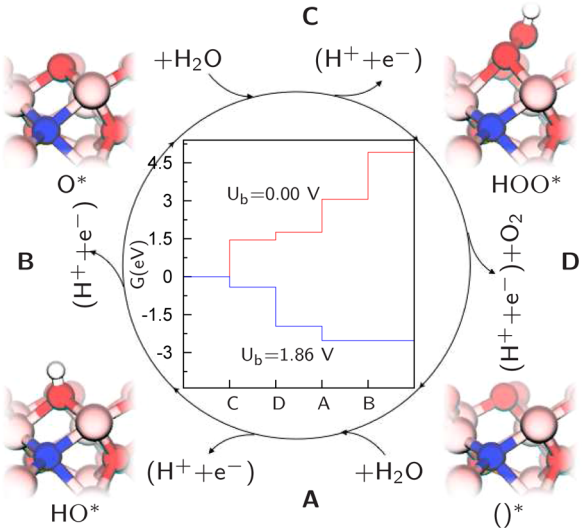

Figure 4. Oxygen evolution at the N-impurity surface.

the PCET sequence is shown with the C → D → A → B order. B is the most energy-demanding step, as on the ideal surface, followed by C. Their reaction free energy is 1.86 and 1.45 eV, respectively. Step A costs 1.30 eV, and the least demanding step is step D, with a free energy cost of 0.31 eV. Here, again we see that B is the overpotential-determining step, requiring an external bias of 0.63 V to allow the oxidation process to become downhill. Again, the change of the reaction free energy with respect to the defect-free surface case is connected to the defect-induced relative stability and the amount of electrons gained by the O atom of O, OH, and OOH species at the surface.

Considering the ideal and N-doped surfaces, the adsorption energy of O is almost the same, and the Bader atomic charges on this atom show a small variation induced by the dopant (see Table 2). The effect on the adsorption energy of the OH intermediate, on the other hand, is more substantial, with a destabilization of about 0.2 eV with respect to the pristine surface. We note that the partial charge of N in the O*, HO*, HOO*, and ()* is −1.03, −0.97, −1.09, and −1.13 $|e^-|$, respectively, compared to −1.10, −1.12, −1.13, and −1.13 $|e^-|$ of the O counterpart in the defect-free case. The most pronounced difference appears to be in the case of the HO* intermediate. The origin of this effect could therefore be linked to the different electrostatic interaction between the OH group and the N atom, compared to the case of the pristine surface. The overall effect is a reduction of the free energy cost of the HO* → O* step (B). The OOH adsorbate becomes less stable on this defective surface, resulting in the higher reaction free energy in step C, with respect to the ideal surface.

3.4. Discussion. We have seen that photo-oxidation of water on hematite surfaces is significantly affected by the presence of defects. Looking at the most demanding step among the four PCET steps in eq 1, our results show that the presence of O-vacancies and N-doping lowers the overpotential, while the presence of Fe-vacancies has the opposite effect. These effects are related to the way the O, OH, OOH intermediates bind to the substrates, namely, these species are singly coordinated to Fe in the presence of a metal vacancy, doubly coordinated, otherwise. This results in different binding geometries as well as in different amounts of electrons gained by the O atoms in the adsorbates.

The partial charge on Fe atoms in the presence of Fe vacancies is higher than the corresponding value for the pristine surface, (see values of $q_Y/()^*$, Table 2), while that induced by the O vacancy or N substituent is lower. This in turn will also affect the partial charge on neighboring O atoms.

In our previous work,[12] we showed that the $O_3 - Fe - O_3-$ surface does not oxidize water efficiently, because it requires an exceedingly high overpotential of 1.22 V. On this oxygen-terminated substrate, each oxygen atom in the outermost layer, which serves as O*, binds to only one iron site. Single iron coordinated oxygen atoms in this work also lead to high overpotential. The reason for this is the nonoptimal adsorption energy of the O adsorbate in this configuration, which turns out to be weakly bonded, leading to an increase in step B.

The overpotential in the case of oxygen vacancy is 0.56 V compared to 0.82 V in the defect-free case, while the experimental value is 0.5−0.6 V. Given that realistic hematite electrodes can contain numerous defects at their surfaces, we do not exclude the possibility that, rather than ideal surfaces, defective (in particular, O-vacancy) counterparts are responsible for the actual overpotential measured in experiments. Our results suggest that the role of defects in electrochemical catalytic materials should be considered in greater detail, because their impact can be significant.

Like metal dopants,[4] nonmetal impurities in hematite can be used to improve the overpotential. In fact, Liao et al.[4] have shown that cation and anion doping by substitution of Fe by Si and O by F gives rise to smaller overpotentials. However, these authors considered F substituting an outermost O atom. As mentioned above, this substitution position leads to a less favorable overpotential compared to a deeper position in the case of N doping. The N atom indirectly involves in the interaction of O, OH, OOH species with the iron sites by modifying their (Fe atoms) partial charges.

In the favorable cases of oxygen-vacancies and N-doping, the reaction steps that determine the overpotential are either the dehydrogenation of the OH group (reaction B), or the formation of the OOH group (reaction C), while oxygen production from OOH is never a problem. Also for the ideal surface the difficult step is the dehydrogenation of the OH to O. Even when B is not the most demanding step, still its free energy is only slightly below that of the most demanding step. That is the reason why we find a linear relation between the difference of energy between O and OH and the overpotential (see below).

Rossmeisl et al.[21] have shown by DFT simulations that the binding energy of the O, OH and OOH intermediates are linearly related, resulting in an overall cost for the steps B and C of 3.2 ± 0.2 eV. We have verified that this relation holds approximately also for the systems investigated in our work. In particular, we obtained (i) ideal surface: 2.05 + 1.41 = 3.46 eV, (ii) O vacancy: 1.73 + 1.79 = 3.52 eV, (iii) N dopant: 1.86 + 1.45 = 3.31 eV. In the presence of a Fe vacancy, however, the system investigated does not obey this empirical rule, (iv) Fe vacancy: 2.18 + 0.45 = 2.63 eV. The reason for this discrepancy can be traced in a change of the binding geometry among the various adsorbates. With the presence of an Fe vacancy (X removed), the O, OH, OOH species can bind to only one iron

DOI: 10.1021/cs5017326
ACS Catal. 2015, 5, 715−721

site Y. This is inherently different from the other cases in which these adsorbates bridge the two X and Y iron atoms. The very same effect has also been studied in the recent work by Halck et al.[28]

In Figure 5a, we show the dependence of the overpotential η on the difference of ΔE_O and ΔE_{OH}. The positive slope implies

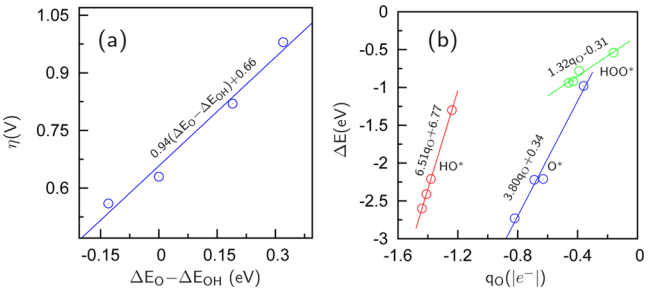

Figure 5. Adsorption energy of O, OH, OOH against partial charge of their O atom (which directly binds to ()*. Partial charges are evaluated with Bader analysis. Solid lines are fitted from computed data.

that the lowest η corresponds to the most negative value of this energy difference. Accept for the Fe-vacancy case, we found that the more negative $\Delta E_O - \Delta E_{OH}$ corresponds to a larger Bader charge at cation iron X in the HO* intermediate. This inverse relation was also found in the case of cation doping.[4] Finally, on the basis of Bader analysis, it was found that the relation between the adsorption energy of O, OH, OOH at the ()* sites and the partial charge of the linking O atom is scaling almost linearly.

Finally, a comment on possible effects of defects on electronic properties of hematite surfaces is added. It is known that defects in a semiconductor can lead to the presence of the so-called gap states. For photovoltaic materials, gap states can directly affect their absorption spectra. Although the influence of gap states of hematite photoanodes on the photocurrent has been addressed in various experiments,[30,31] the catalytic effects of gap states on the stability of water oxidation intermediates is not straightforward to examine experimentally. To see if gap states are induced by O vacancies or N dopants, we have calculated the projected density of states of hematite surfaces, details are included in the Supporting Information. Our calculated data show that the O vacancies or N dopants do not increase number of gap states of the defect-free surface. To a first approximation, O vacancies or N dopants do not induce more gap states. Moreover, with these defects they are still localized at surface oxygen and iron atoms, and their real-space distribution does not change appreciably (see Supporting Information). Note that a higher density of defects may lead to a different picture. However, to have a more serious description of their effects on the light absorption ability, one should consider more accurate methods such as hybrid density functionals which are beyond the scope of this work.

4. SUMMARY

We have investigated the influence of point defects of hematite(0001) surfaces on the photo-oxidation of water using *first-principles* PBE+U calculations. O/Fe vacancies and N substituents were introduced by removing atoms or directly replacing O with the dopants. Apart from the iron vacancies, other defects reduce the overpotential by 0.2−0.3 V. The overpotential increase or decrease was interpreted with the change in the adsorption energy of the O*, HO*, OOH* intermediates, which was found to correlate approximately with the Bader charge on the O atom of the adsorbate. Given the possibility of engineering the type and concentration of point defects in oxide materials, these should be considered as a novel strategy to improve, at the same time, electronic and catalytic functions of hematite in photodriven water splitting.

■ ASSOCIATED CONTENT

Supporting Information

The following file is available free of charge on the ACS Publications website at DOI: 10.1021/cs5017326.

Density of states calculations and local density of states calculations mentioned in the main text (PDF)

■ AUTHOR INFORMATION

Corresponding Author

*E-mail: manhth.nguyen@gmail.com.

Notes

The authors declare no competing financial interest.

■ ACKNOWLEDGMENTS

We acknowledge the CINECA Award H2OSPLIT - HP10B6BMAA, 2013, for the availability of high-performance computing resources and support.

■ REFERENCES

(1) Walter, M. G.; Warren, E. L.; McKone, J. R.; Boettcher, S. W.; Mi, Q.; Santori, E. A.; Lewis, N. S. *Chem. Rev.* **2010**, *110*, 6446−6473.
(2) Sivula, K.; Le Formal, F.; Grätzel, M. *ChemSusChem* **2011**, *4*, 432−449.
(3) Bora, D. K.; Braun, A.; Constable, E. C. *Energy Environ. Sci.* **2013**, *6*, 407−425.
(4) Liao, P.; Keith, J. A.; Carter, E. A. *J. Am. Chem. Soc.* **2012**, *134*, 13296−13309.
(5) Yang, T.-Y.; Kang, H.-Y.; Sim, U.; Lee, Y.-J.; Lee, J.-H.; Koo, B.; K. T. Nam, K. T.; Joo, Y.-C. *Phys. Chem. Chem. Phys.* **2013**, *15*, 2117−2124.
(6) Ashcroft, N. W.; Mermin, N. D. *Solid State Physics*, 1st ed.; Cengage Learning: Stamford, CT, 1976.
(7) Wendt, S.; Schaub, R.; Matthiesen, J.; Vestergaard, E. K.; Wahlström, E.; Rasmussen, M. D.; Thostrup, P.; Molina, L. M.; Lægsgaard, E.; Stensgaard, I.; Hammer, B.; Besenbacher, F. *Surf. Sci.* **2005**, *598*, 226−245.
(8) Hammer, B.; Nørskov, J. K. *Adv. Catal.* **2000**, *45*, 71−129.
(9) Nguyen, M.-T.; Seriani, N.; Gebauer, R. *ChemPhysChem* **2014**, *15*, 2930−2935.
(10) Liao, P.; Toroker, M. C.; Carter, E. A. *Nano Lett.* **2011**, *11*, 1775−1781.
(11) Pradhan, G. K.; Sahua, N.; Parida, K. M. *RSC Adv.* **2013**, *3*, 7912−7920.
(12) Nguyen, M.-T; Seriani, N.; Piccinin, S.; Gebauer, R. *J. Chem. Phys.* **2013**, *140*, 064703.
(13) van de Krol, R.; Grätzel, M. *Photoelectrochemical Hydrogen Production*; Springer: New York, 2012.
(14) Perdew, J. P.; Burke, K.; Ernzerhof, M. *Phys. Rev. Lett.* **1996**, *77*, 3865−3868.
(15) Anisimov, V. I.; Zaanen, J.; Andersen, O. K. *Phys. Rev. B* **1991**, *44*, 943−954.
(16) Giannozzi, P.; Baroni, S.; Bonini, N.; Calandra, M.; Car, R.; Cavazzoni, C.; Ceresoli, D.; Chiarotti, G. L.; Cococcioni, M.; Dabo, I.; Dal Corso, A.; Fabris, S.; Fratesi, G.; de Gironcoli, S.; Gebauer, R.; Gerstmann, U.; Gougoussis, C.; Kokalj, A.; Lazzeri, M.; Martin-Samos, L.; Marzari, N.; Mauri, F.; Mazzarello, R.; Paolini, S.; Pasquarello, A.; Paulatto, L.; Sbraccia, C.; Scandolo, S.; Sclauzero, G.; Seitsonen, A. P.;

DOI: 10.1021/cs5017326
ACS Catal. 2015, 5, 715−721

Smogunov, A.; Umari, P.; Wentzcovitch, R. M. *J. Phys.:Condens. Matter* **2009**, *21*, 395502.
(17) Liao, P.; Carter, E. A. *Phys. Chem. Chem. Phys.* **2011**, *13*, 15189−15199.
(18) Vanderbilt, D. *Phys. Rev. B* **1990**, *41*, 7892−7895.
(19) Walker, B.; Gebauer, R. *J. Chem. Phys.* **2007**, *127*, 164106.
(20) Nguyen, M.-T.; Seriani, N.; Gebauer, R. *J. Chem. Phys.* **2013**, *138*, 194709.
(21) Rossmeisl, J.; Qu, Z.-W.; Zhu, H.; Kroes, G.-J.; Nørskov, J. K. *J. Electroanal. Chem.* **2007**, *607*, 83−89.
(22) Nørskov, J. K.; Rossmeisl, J.; Logadottir, A.; Lindqvist, L.; Kitchin, J. R.; Bligaard, T.; Jónsson, H. *J. Phys. Chem. B* **2004**, *108*, 17886−17892.
(23) Hellman, A.; Pala, R. G. S. *J. Phys. Chem. C* **2011**, *115*, 12901−12907.
(24) Valdés, Á.; Kroes, G.-J. *J. Chem. Phys.* **2009**, *130*, 114701.
(25) Bader, R. F. W. *Atoms in Molecules − A Quantum Theory*; Oxford University Press: Oxford, 1990).
(26) Tang, W.; Sanville, E.; Henkelman, G. *J. Phys.: Condens. Matter* **2009**, *21*, 084204. see also: http://theory.cm.utexas.edu/bader/
(27) Brillet, J.; Cornuz, M.; Le Formal, F.; Yum, J. H.; Grätzel, M.; Sivula, K. *J. Mater. Res.* **2010**, *25*, 17−24.
(28) Halck, N. B.; Petrykin, V.; Krtil, P.; Rossmeisl, J. *Phys. Chem. Chem. Phys.* **2014**, *16*, 13682−13688.
(29) Iandolo, B.; Hellman, A. *Angew. Chem., Int. Ed.* **2014**, *53*, 13404−13408.
(30) Klahr, B.; Gimenez, S.; Fabregat-Santiago, F.; Hamann, T.; Bisquert, J. *J. Am. Chem. Soc.* **2012**, *134*, 4294−4302.
(31) Klahr, B.; Hamann, T. *J. Phys. Chem. C* **2014**, *118*, 10393−10399.

DOI: 10.1021/cs5017326
ACS Catal. 2015, 5, 715−721